Atmos. Meas. Tech. Discuss., doi:10.5194/amt-2016-271, 2016
Manuscript under review for journal Atmos. Meas. Tech.
Published: 12 September 2016

Atmospheric Measurement Techniques Discussions

Collection efficiency of α-pinene secondary organic aerosol particles explored via light scattering single particle aerosol mass spectrometry

Ellis Shipley Robinson[1,2], Timothy B. Onasch[3], Douglas Worsnop[3], and Neil M. Donahue[1,2]

[1]Carnegie Mellon University Center for Atmospheric Particle Studies, Pittsburgh, PA, USA
[2]Department of Chemical Engineering, Carnegie Mellon University, Pittsburgh, PA, USA
[3]Aerodyne Research, Inc., Billerica, MA, USA

Correspondence to: N.M. Donahue
(nmd@andrew.cmu.edu)

Abstract.

We investigated the collection efficiency and effective ionization efficiency for secondary organic aerosol (SOA) particles made from α-pinene + O_3 using the single-particle capabilities of the Aerosol Mass Spectrometer (AMS). The mean count-based collection efficiency (CE_p) for SOA across these experiments is 0.30 ($\pm$0.04 S.D.), ranging from 0.25 to 0.40. The mean mass-based collection efficiency (CE_m) is 0.49 ($\pm$0.07 S.D.). This sub-unit collection efficiency and delayed vaporization is attributable to particle bounce in the vaporization region. Using the coupled optical and chemical detection of the light scattering single-particle (LSSP) module of the AMS, we provide clear evidence that "delayed vaporization" is somewhat of a misnomer for these particles: SOA particles that appear within the chopper window do not vaporize at a slow rate; rather, they flash-vaporize, but often not on the initial impact with the vaporizer, and instead upon a subsequent impact with a hot surface in the vaporization region. We also find that the effective ionization efficiency (defined as ions per particle, IPP) decreases with delayed arrival time. CE_p is not a function of particle size (for the mobility diameter range investigated, 170-460 nm), but we did see a decrease in CE_p with thermodenuder temperature, implying that oxidation state and/or volatility can affect CE_p for SOA.

1 Introduction

Organic aerosol (OA) comprises a significant fraction of submicron atmospheric particulate mass, ranging from 20-90% (Kanakidou et al., 2005; Jimenez et al., 2009). OA has been shown to have

Atmos. Meas. Tech. Discuss., doi:10.5194/amt-2016-271, 2016
Manuscript under review for journal Atmos. Meas. Tech.
Published: 12 September 2016

Atmospheric Measurement Techniques Discussions

negative impacts on human health (e.g. Lozano et al., 2013) and remains highly uncertain in its effect on radiative climate forcing (e.g. Solomon et al., 2007). The physical and chemical characteristics of OA can vary dramatically, and depend strongly on source, location, atmospheric age, and other factors. Despite the ubiquity and importance of OA, real-time measurements are technically challenging due to the wide range of chemical composition, particle size, and volatility represented by OA in the atmosphere.

The Aerosol Mass Spectrometer (AMS, Aerodyne Research, Inc.) is used widely in both ambient and laboratory measurements of OA. It has enabled significant advances in our understanding of how organic aerosols form (Craven et al., 2012), age (Aiken et al., 2008), and mix, (Robinson et al., 2013) by providing real-time measurements of size-resolved composition and mass for submicron, non-refractory particulate matter (NR-PM_1). However, a lingering challenge with full quantification of NR-PM_1 in the AMS is the mass collection efficiency (Canagaratna et al., 2007), which is the ratio of the measured AMS mass signal to the actual NR-PM_1 mass concentration. Another factor influencing calibration of the AMS mass response is the species-specific relative ionization efficiency (RIE) of analyte; this is relative to a calibrant, typically ammonium nitrate. However, this value is assumed to be roughly similar for all organic species (Jimenez et al., 2003), and is not subject to matrix effects. To obtain quantitative agreement between the AMS and other collocated instruments in field campaigns, a mass collection efficiency (CE_m) is usually applied to correct for the consistently lower AMS-measured mass. CE_m can be written as:

$$CE_m = \frac{S_{AMS}}{S_O} \quad (1)$$

where S_{AMS} is the signal from the AMS and S_O is the signal of the another (perfectly calibrated) instrument. Importantly, this calculation assumes ideal operating conditions for both instruments and the application of all other appropriate correction factors. For example, Drewnick et al. (2003), in a sulfate aerosol intercomparison study, applied a scaling factor of 2.41 (CE_m = 0.42) to the AMS-measured sulfate to achieve good agreement with a collocated particle into liquid sampler (PILS) instrument. In another example, Middlebrook et al. (2012) recently reported parameterizations of CE_m for ambient sulfate-containing particles that could be used to predict CE_m based on particle acidity and mass fraction of ammonium nitrate. High CE_m values were consistent with predicted liquid phase-state at 298 K. Thus, CE_m should be thought of as a sensitivity factor that varies for particle types with different compositions and phase-states.

Huffman et al. (2005) define CE_m as the product of three, size-dependent terms:

$$CE_m(d_{va}) = E_L(d_{va}) \times E_S(d_{va}) \times E_B(d_{va}) \quad (2)$$

where $E_L(d_{va})$ is the lens transmission efficiency as a function of aerodynamic diameter, (d_{va}); $E_S(d_{va})$ is the striking efficiency of particles on the AMS vaporizer transmitted through the lens to the time-of-flight chamber; and $E_B(d_{va})$ is the vaporization efficiency of particles that strike the vaporizer

Atmos. Meas. Tech. Discuss., doi:10.5194/amt-2016-271, 2016
Manuscript under review for journal Atmos. Meas. Tech.
Published: 12 September 2016

Atmospheric Measurement Techniques Discussions

surface, also known as "bounce" because particles can bounce away from the vaporizer surface and escape detection. Any particle that enters the instrument, but is not detected by the mass spectrometer due to any of these three loss terms contributes to the mass discrepancy between the AMS and another (perfectly-calibrated) mass measurement.

Previous measurements and models have characterized the loss of particles in the lens region and orifice, and have shown near-unit transmission efficiencies for particles in the size-range of 60-600 nm. However, for particle populations whose distribution is significantly outside of the transmission window, especially for larger particles, E_L can contribute significantly to CE_m (Quinn et al., 2006). The striking efficiency is a measurement of the divergence of the particle beam upon expansion into the time-of-flight (ToF) chamber. While spherical particles can be narrowly focused on the 3.8 mm-wide vaporizer over the distance of the ToF chamber, non-spherical particles can diverge from the focused beam, causing sub-unit values of E_S (Huffman et al., 2005). Studies show this term accounts for very little particle loss for ambient aerosol (Salcedo et al., 2007), as well as laboratory SOA and $(NH_4)_2SO_4$ (Docherty et al., 2013). E_S can be well-characterized by the use of a beam-width probe (Huffman et al., 2005).

In the majority of cases, the largest uncertainty and largest contributor to sub-unit CE_m is the particle bounce term, E_B. Particle bounce has long been known to confound particle measurements, such as impactors and surface-desorption mass spectrometers (e.g Myers and Fite, 1975; Virtanen et al., 2010). A limited number of studies have investigated the nature and root cause of particle bounce for laboratory aerosols in the AMS. Alfarra (2004) identified particle phase-state as a controller of particle bounce for a selection of laboratory organics, where particle phase state was inferred from the room temperature properties of the bulk materials. Liquid particles had near-unit CE_m, while solid particles had much lower efficiencies ($CE_m = 0.2$ to 0.5). Matthew et al. (2008) found phase state to govern particle bounce as well. Ammonium nitrate particles, thought to be metastable liquids at their experimental conditions (Lightstone et al., 2000), displayed high CE_m, while dry ammonium sulfate particles had CE_m = 0.22, which increased to 0.73 when the particles were hydrated and deliquesced. Matthew et al. (2008) also found that CE_m for dry ammonium sulfate increased as the thickness of a liquid dioctyl sebacate coating layer increased. In some chamber experiments, Bahreini et al. (2005) showed this same increase in CE_m for dry ammonium sulfate particles with condensation of an SOA layer. However, for other SOA experiments, CE_m for ammonium sulfate seed particles actually decreased with the condensation of SOA, implying that the SOA phase-state was highly variable in their experiments and/or that other factors also govern particle bounce in the AMS, such as compositon or volatility. Similarly, Robinson et al. (2015) showed that CE of liquid squalane (CE $\sim$1) particles decreased following SOA condensation. Docherty et al. (2013) report an inverse relationship between CE_m for chamber-generated SOA and the f_{44}/f_{57} ratio (where *m*/z 44 and *m*/z 57 are comprised almost solely of signals from CO_2^+ and $C_4H_9^+$, and f_i is the fraction of (m/z_i) to the total organic signal). This implicates oxidation state as either a factor influencing CE_m,

Atmos. Meas. Tech. Discuss., doi:10.5194/amt-2016-271, 2016
Manuscript under review for journal Atmos. Meas. Tech.
Published: 12 September 2016

Atmospheric Measurement Techniques Discussions

or as a proxy variable for what makes a particle bouncy.

An even smaller number of studies have used the light scattering single-particle (LSSP) module of the AMS to investigate collection efficiency, despite its ability to provide a real-time, particle number-based measurement of E_B. When E_S and $E_L \sim 1$, collection efficiency is equal to the bounce efficiency ($CE \sim E_B$) We denote this number-based collection efficiency as CE_p for "particle collection efficiency," which is defined as:

$$CE_p = \frac{\text{Particles with ion signal above threshold}}{\text{All particles}} \quad (3)$$

Cross et al. (2007) first introduced LSSP as a method to resolve real-time densities of externally-mixed aerosols. Cross et al. (2009) later described the ability of LSSP to measure CE_p for ambient particles from Mexico City, and found that a significant fraction of the optically-detected particles were either undetected by the mass spectrometer due to bounce (hereto referred to as "null") or exhibited signal at a time much later than would be expected based on their *in situ* measured velocity (referred to as "delayed"). "Prompt" particles, those that gave an appreciable chemical ion signal when they were expected to, made up only 23% of the measured aerosol, with the delayed fraction at 0.26 and the null fraction at 0.51. Liu et al. (2013) also report CE_p for ambient measurements taken in Bakersfield, CA (Cal-Nex). They report a 0.46 prompt fraction, 0.06 delayed, and 0.48 null, and found a slight size-dependence in the campaign-average CE_p, which exhibited a maximum around d_{va} = 600 nm (0.52) and a minimum (0.42) for large particles. Slowik et al. (2009) compared CE_m (density-corrected SMPS/AMS comparison) and CE_p for an ambient biogenic SOA event, and found them to be equal.

Here we further explore the use of LSSP to identify the nature of collection efficiency for lab and chamber-generated aerosols. We quantify particle bounce for SOA from α-pinene ozonolysis, as well as ammonium nitrate, ammonium sulfate, and squalane. We illustrate the difference between mass-based and number-based CE, which are not necessarily the same even for monodisperse aerosol, due both to decreasing effective ionization efficiencies for delayed particles (defined as ions per particle or IPP) and mass that registers at the detector on timescales much longer than the chopper cycle. We show that IPP decreases with delay time, that CE_p is not a function of size for the SOA in this study, and that low volatility and/or high oxidation state decreases CE_p for SOA.

2 Methods

2.1 Particle generation and sampling

We prepared inorganic aerosols (ammonium nitrate, ammonium sulfate) by atomizing dilute solution (1 g/L) using a constant output nebulizer (aerosol generator model 3076; TSI, Inc.). We sent these particles through a krypton neutralizer (10 mC), then size-selected them using a differential mobility

Atmos. Meas. Tech. Discuss., doi:10.5194/amt-2016-271, 2016
Manuscript under review for journal Atmos. Meas. Tech.
Published: 12 September 2016

Atmospheric Measurement Techniques Discussions

analyzer (DMA; classifier model 3080; TSI, Inc.) before sampling.

We sampled size-selected SOA in this same manner, but with a different preparation procedure. We injected a 1.2 μL aliquot of α-pinene (Sigma Aldrich, $>$99%) into a clean and dry (RH$<$ 3%) 100-L Tedlar sample bag (SKC, Inc.) at an estimated mixing ratio of ($\sim$ 2 ppm) and charged the bag with excess ozone. This SOA formed at a high concentration ($C_{OA} \approx 1500$ μg m^{-3}). This allowed us to study homogeneously nucleated SOA with the single-particle capability of the AMS, as the scattering laser requires large ($d_{va} \geq 180$ nm) particles. See Figure 1 for the general experimental schematic.

We produced squalane aerosols directly in the 12 m^3 Carnegie Mellon University smog chamber, described elsewhere in greater detail (e.g. Robinson et al., 2015). In brief, we flushed the smog chamber continuously for $>$12 h with clean, dry air (cleaned with HEPA, silica-gel, and activated-carbon filters in series) to ensure low background particle, organic vapor, and water vapor concentrations. We prepared squalane particles by flash vaporization using a small, resistive stainless-steel heater. We placed a small aliquot of squalane (0.75 μL) on the heater surface, which we then inserted into the smog chamber. Clean dispersion air flowed through the heater to carry and mix the squalane plume into the chamber while we power-cycled the heater for 10 minutes. Pure squalane particles formed as the vapor plume cooled.

We measured ensemble particle volume and number concentrations using a Scanning Mobility Particle Sizer (SMPS; TSI, Inc.). We measured ensemble composition and mass with the High-Resolution Aerosol Mass Spectrometer (HR-Tof-AMS; Aerodyne, Inc,) operated in single-reflectron V-mode, fully described by DeCarlo et al. (2006). We acquired single-particle mass spectra using the light-scattering single-particle (LSSP) module coupled to the HR-ToF-AMS. We analyzed single-particle AMS data using Sparrow 1.04D[1], and ensemble AMS composition data using SQUIRREL 1.51[2].

2.2 Operation of light-scattering module

The LSSP module has been described in detail elsewhere in the literature (Cross et al., 2009). Briefly, the LSSP module consists of a continuous-wave laser (405 nm, 50-mW; LC BCL-050-405; Crysta-Laser) that crosses the collimated particle beam within the time-of-flight region of the AMS. Scattered light from sampled particles is collected by an ellipsoidal mirror that focuses the light onto a photomultiplier tube. This light-scattering signal constrains the particle's velocity between the opening of the AMS chopper and the laser, allowing for the calculation of the vacuum aerodynamic diameter. It also prompts collection of individual mass spectra over the entire chopper cycle (e.g. 200 spectra/chopper), allowing for the identification of signals from individual particles within the

[1]Sparrow 1.04A,written by D. Sueper, Aerodyne Research Inc. and University of Colorado at Boulder; available at http://cires.colorado.edu/jimenez-group/ ToFAMSResources/ToFSoftware/index.htmlAnalysis4

[2]SQUIRREL 1.51,written by D. Sueper, Aerodyne Research Inc. and University of Colorado at Boulder; available at http://tinyurl.com/tofams?analysis

Atmos. Meas. Tech. Discuss., doi:10.5194/amt-2016-271, 2016
Manuscript under review for journal Atmos. Meas. Tech.
Published: 12 September 2016

full chopper cycle. Saving at this data rate without the laser triggering (meaning all chopper cycles, not just ones containing particles) is not practically useful, as it results in an unmanageable data load. For example, when Drewnick et al. (2005) collected ToF-AMS single-particle data without any triggering mechanism, of the 2.41 GB of data they collected, only 4 MB represented meaningful single-particle spectra after applying their thresholding algorithm. The LSSP enables continuous single-particle detection at a high duty cycle for the long timescales of chamber studies or ambient sampling.

For data processing, we used an operationally-defined light-scattering threshold of five (signal-to-noise, S/N) to identify particle events, and a mass threshold of six ions to identify a detected particle to be further considered for particle classification, similar to Liu et al. (2013). For ammonium sulfate, ammonium nitrate, and SOA, we used Sparrow's default ion list (*m/z* 15, 30, 35, 36, 41, 43, 46, 48, 55, 57, 64, 71, 73, 80, 81, 98) for identifying particle events in the mass spectra of each chopper cycle. We used a different list of deuterated ions (*m/z* 48, 50, 66, 82, 98) to identify MS events for d_{62}-squalane particles. We processed a subset of SOA experiments with an adjusted ion list based on the 13 highest-signal ions for SOA that do not have significant background interferences identified with MS mode spectra (*m/z* 15, 26, 27, 29, 41, 42, 43, 44, 53, 55, 65, 67, 69, 79), but our collection efficiency results were not sensitive to this change.

At the number concentrations of the high-C_{OA} SOA experiments, coincident particles—multiple particles sampled in a single chopper cycle—were present (13% of particles were coincident), but identifiable from the scattered light signal. For typical smog chamber and ambient number concentrations (e.g. $\leq$ 2,000 cm^{-3}), the probability for coincidence is rare. We expect $\sim$ 1 particle per chopper cycle for a 1% chopper slit ($\sim$ 70 μs wide) at typical conditions. We filtered out coincident particles (identified by multiple instances where the light scattering S/N >5 during a single chopper cycle) using the Sparrow analysis program and we did not consider them in our analysis or calculation of CE_p.

2.3 Calculation of collection efficiency

We classified individual particle events based on how they interacted with the vaporizer, both in terms of their effective ionization efficiency and vaporization quickness. As defined in Cross et al. (2009), particles categorized as "prompt" arrive at the mass detector within a narrow time range after they would be expected to arrive based on their measured velocity in the ToF region and assuming instantaneous vaporization/ionization. The operationally-defined boundary between the prompt and delayed particles is when the actual arrival of the mass signal differs from the expected arrival time by 20% or more. In other words, we compared the measured arrival time at the detector ($MS_{arrival}$) and the LS-estimated arrival time ($LS_{arrival}$) based on the measured velocity between the chopper and laser to draw the boundary between prompt particles ($MS_{arrival}/LS_{arrival}$ <1.2) and delayed particles ($MS_{arrival}/LS_{arrival}$ >1.2). As we shall show, this particular value for determining the boundary between prompt

Atmos. Meas. Tech. Discuss., doi:10.5194/amt-2016-271, 2016
Manuscript under review for journal Atmos. Meas. Tech.
Published: 12 September 2016

Atmospheric Measurement Techniques Discussions

and delayed particles is arbitrary.

LSSP provides an internal number-based measure of the AMS collection efficiency (Cross et al., 2009). The wide laser beam (≈ 2 mm), relative to the width of the particle beam (≈ 0.5 mm), allows for near complete optical detection of particles above the detection limit of the laser (d_{va} >180 nm). The LSSP-based CE_p is the comparison between the optically-detected particles (i.e. all particles that enter the TOF region and that will hit the vaporizer surface) and the number of particles that are chemically-detected (i.e. give signal in the mass spectrometer). For all particles sampled here, E_S and E_L are reasonably assumed to be 1. Thus, in terms of the categories prompt, delayed, and null, the general definition of CE_p from equation 3 can re-written as:

$$CE_p = \frac{N_{prompt} + N_{delayed}}{N_{prompt} + N_{delayed} + N_{null}} \quad (4)$$

where e.g. N_{prompt} is the number of prompt particles. In this formulation, we consider both prompt and delayed particles as those that give meaningful chemical signals at the detector, though it may be of interest in other studies to look at the CE_p from e.g. only prompt particles. We are equating CE_p with E_B, a reasonable assumption for the aerosols studied here as they all fall within the lens transmission window (E_L = 1) and are spherical (Zelenyuk et al. (2008)) and therefore do not exhibit significant divergence from the particle beam (E_S= 1). However, it is important to note this collection efficiency accounts only for whether or not a particle was observed in the mass spectrometer, and does not account at all for signal strength above the detection threshold.

3 Results and Discussion

3.1 Delayed vaporization PToF artifact

It is standard practice to present comparisons between the mass-weighted size distribution from the SMPS and the particle time-of-flight mass distribution from the AMS to compute density and collection efficiency (DeCarlo et al., 2004; Kostenidou et al., 2007; Shilling et al., 2009). The SMPS size-distribution is multiplied by the density to align the mode diameters according to,

$$d_{va} = \frac{\rho_p}{\rho_0} \frac{d_{ve}}{\chi} \quad (5)$$

where ρ_p is particle density, ρ_0 is standard density (1 g cm^{-3}), and χ is the dynamic shape factor, which is equal to one for spherical particles and is assumed to be true in the case of SOA from α-pinene ozonolysis (Zelenyuk et al., 2008). For spherical particles, d_{ve}, the volume equivalent diameter, is equal to mobility diameter.

For this example experiment, where 370 nm SOA particles were size-selected using a DMA, shown in Figure 2, we estimate the density to be 1.1 g/cm^3 from aligning the AMS and SMPS mass distribution mode diameters. The shaded blue area is the frequency of optically-counted particles

Atmos. Meas. Tech. Discuss., doi:10.5194/amt-2016-271, 2016
Manuscript under review for journal Atmos. Meas. Tech.
Published: 12 September 2016

as a function of size, as measured by light-scattering in the AMS. Like the SMPS distribution, this histogram is tight, as we expect it to be for size-selected particles. However, even after shifting the SMPS distribution by the density, the agreement between the SMPS- and AMS-derived mass distributions degrades considerably at large diameters.

We explore the nature of the divergence between the AMS PToF mass distribution and the SMPS-derived mass distribution at large apparent diameters using data from LSSP mode. We show the flight path, and resulting data, for a particle in the LSSP-AMS in Figure 3 (similar to Figure 7 in Cross et al., 2009). The scattered light pulse (magenta trace) triggers acquisition of mass spectra over the entire chopper cycle. Individual extractions from the mass spectrometer, which are usually averaged together over tens of seconds to minutes, are resolved at $\sim$30 μs (the ToF-MS pulser period) in single-particle mode (orange trace). Using the distance between the chopper and the point of intersection between the laser and particle beams, a flight velocity is calculated and used to predict the arrival of the particle's ions at the mass detector, assuming instantaneous vaporization and ionization. We show the mass signal as a function of time-of-flight for the chopper cycle in orange. For some particles, the arrival of the ions at the detector is significantly offset ("delayed") from the predicted arrival time. This offset (labeled "δ" in Figure 3) is used to categorize particles into prompt and delayed categories, further discussed in Section 2.3.

Figure 4 shows total ion signals from individual particles (grey circles) along with total summed signals of prompt (blue) and delayed (red) particles as a function of time-of-flight. We see that the large-diameter PToF tail (green) matches the delayed particle distribution. Additionally, none of the prompt particles have measured times-of-flight greater than 4 ms. As described in Cross et al. (2009) for ambient OOA measured in Mexico City, the physical basis for the broadened PToF distribution at large diameters is particles with delayed vaporization, which comprise a significant fraction of the measured single particles in this SOA experiment (19% of all particles). However, the mechanism of the delayed vaporization has not yet been fully described for SOA from α-pinene + O_3.

3.2 Collection efficiency

The average CE_p across all experiments was 0.30 ($\pm$0.04), while the average CE_m was 0.49 ($\pm$0.07). We calculated CE_m using equation 1, where S_{AMS} is the AMS-measured mass from MS mode and S_o is the density-corrected SMPS-measured mass. Like Cross et al. (2009), we see that $CE_m > CE_p$, which likely reflects two differences between the mass-based and particle-based collection efficiencies. First, by definition, null particles in LSSP mode, those which do not register mass above the 6 ion threshold, provide no chemical information. LSSP can only tell us that these particles bounced away from the vaporizer. However, there are examples (e.g. Huffman et al., 2009) where particulate mass is detected by the AMS on very long timescales (5 s) compared to the length of the chopper cycle window (5 ms). While a particle defined as "null" provides no chemical information whatsoever in LSSP mode, it is likely that not all null particles are created equal: some bounce away from the

Atmos. Meas. Tech. Discuss., doi:10.5194/amt-2016-271, 2016
Manuscript under review for journal Atmos. Meas. Tech.
Published: 12 September 2016

Atmospheric Measurement Techniques Discussions

vaporization/ionization region altogether and are not measured at all, while some bounce from the vaporizer cone but still do evaporate at very long timescales relative to the chopper cycle. Evidently, the sum of some number of these particles from the null category do result in detectable mass on timescales longer than the chopper cycle, as evinced by CE_m being significantly greater than CE_p.

Secondly, some particles that would register mass above the LSSP threshold may be delayed such that their mass signal registers at the detector just beyond the chopper cycle. As depicted in Figure 4, the delay times for some particles are just beyond the chopper cycle window that we used for these experiments, as there are still mass signals arriving at the very right edge of the plot where the cycle ends. For aerosol types with a high delayed fraction like this SOA, a longer chopper-cycle would better accommodate these particles with long (2 ms) delay times. Thus, while LSSP provides an *in situ* measurement of the AMS collection efficiency, it is important to distinguish between the LSSP-based (eqn. 4) and mass-based (eqn. 1) calculations of collection efficiency.

3.3 Delayed particle signal strengths

Despite nearly equal numbers of prompt (17% of all particles) and delayed particles (19% of all particles) for this SOA, these two particle categories do not contribute equal mass signal to the detector. As shown in Figure 5, prompt particles produce significantly more signal per particle than delayed particles even though they are all the same size. We plot in Figure 5 a histogram of ions per particle (IPP), normalized so that the sum of the bins for each category is one. This figure shows that the effective ionization efficiency for prompt particles is higher than that of delayed particles. Note that this "effective" ionization efficiency is not only a function of the ionization efficiency of the molecules being ionized by the 70 eV source (a molecular property), but also convolves the instrument sensitivity to particles that may be vaporized in a sub-optimal location (for ion extraction). If delayed and prompt particles had the same IPP, the delayed vaporization tail in the AMS mass distribution for SOA shown in Figure 2 would be even more pronounced.

The single-particle mass signal (IPP) is a smooth function both within the prompt and delayed categories, possibly providing reason to redefine what it means to be "prompt" vs "delayed." Figure 6 shows a steady decrease in the average IPP as a function of delay time for delays shorter than 1 ms. For delay times longer than 1 ms, the IPP is constant with delay time. The error bars represent the standard error of the mean within each bin, while the gray shadow shows the standard deviation for each bin reflecting the inherent spread of single-particle mass signals. For comparison, we include on the plot the average IPP value across all prompt and delayed particles, which is very similar to its calculated value based on the calibration ionization efficiency (IE) and the default relative IE (RIE) value for organics of 1.4. It should be noted here that, as is done in most analysis of AMS data, converting from the nitrate-equivalent mass to the absolute mass measurement for a given non-refractory species (e.g. organics, sulfate, chloride, etc.) requires the application of both a species-specific values of CE as well as RIE (see e.g. equations 3.8 and 3.9 in Alfarra, 2004).

Atmos. Meas. Tech. Discuss., doi:10.5194/amt-2016-271, 2016
Manuscript under review for journal Atmos. Meas. Tech.
Published: 12 September 2016

Thus, any measurement of CE also has inherent value into understanding RIE for a given species. Figure 6 illustrates this, as the measured average IPP for all particles matches the calculated value. However, clearly the least and most delayed particles have IPPs much different than the average, and thus particle bounce the associated loss of signal significantly affects IPP for a given particle. Measurements of RIE for various species using the AMS, as have been reported by e.g. Mensah et al. (2011) and Silva et al. (2008), is only possible when CE for the sampled aerosol particles is well-known. Given that LSSP measures CE inherently, easier and more routine measurements of species-specific RIE values, especially in ambient datasets, should be made possible with application of the LSSP module.

Plotting the accumulated particle counts as a function of delay time shows how single-particle information from LSSP mode can be used to best understand the response of the AMS to different particle types, each with its own sensitivity in the instrument (Figure 7). We scale the traces in Figure 7a by their measured CE_p values (from equation 4). The effect of delay time on IPP is absent for ammonium nitrate, the standard mass calibrant for the AMS, because all particles arrive within the first few delay time bins. Squalane, a liquid at room temperatures with a near-unit CE_p, largely accumulates its signal at small delay times, but is noticeably slower to do so than ammonium nitrate. This is likely attributable both to the lower volatility of squalane and to the larger molecular weight of squalane (423 g/mol) compared to ammonium nitrate (80 g/mol). We estimate the squalane vapor pressure using SIMPOL (Pankow and Asher, 2008), and use the ammonium nitrate vapor pressure reported by Richardson and Hightower (1987)): Ammonium nitrate is more volatile than squalane ($\sim 30\ \mu g\ m^{-3}$ and $\sim 0.1\ \mu g\ m^{-3}$, respectively). Saleh et al. (2016) calculated the differences in evaporation timescales in the AMS vaporizer for species of different volatility, while Murphy (2015) discuss the molecular weight dependence on the movement of ions from the ion source to the ion optics region in a free molecular regime. Unlike both ammonium nitrate and squalane, however, SOA exhibits delayed vaporization and low CE_p, similar to crystalline ammonium sulfate, a possible indication of a solid or semi-solid phase state, extremely low-volatility material, or both.

Figure 7b shows how the total mass signal from single SOA particles accumulates faster than the particle counts as a function of delay time, as particles with low delay times contribute relatively more mass signal on average. The accumulation of single-particle counts is scaled by CE_p, while the single-particle mass accumulation trace is scaled by CE_m. We use $CE_m^{'}$ to denote the mass collection efficiency calculated by comparing the AMS PToF vs SMPS mass, and CE_m to denote the mass collection efficiency calculated according to equation 1. The difference between $CE_m^{'}$ and CE_m is the amount of mass that can be attributed particles counted as null by LSSP but are detected in MS mode at timescales much longer than the chopper cycle.

Atmos. Meas. Tech. Discuss., doi:10.5194/amt-2016-271, 2016
Manuscript under review for journal Atmos. Meas. Tech.
Published: 12 September 2016

Atmospheric Measurement Techniques Discussions

3.4 Nature of particle-vaporizer interactions

These results seem to indicate that when an aerosol type exhibits bounce, it also exhibits delayed vaporization and thus lower effective ionization efficiency for some fraction of particles. In investigating the offset between expected and actual arrival times, we tested two ideas about how the signal at the mass detector would arrive for SOA within the LSSP chopper cycle. If an SOA particle strikes and sticks to the vaporizer surface, but does not promptly vaporize, it should show an accumulation of mass at the detector over time, beginning at the expected arrival time. It should sizzle. However, if the particle bounces off the vaporizer without any significant evaporation, and somehow returns to a hot surface at a later time, then the time-resolved arrival of ions should look similar to a prompt particle that vaporizes upon impact, albeit after some time associated with its bouncy journey.

Indeed, when the mass arrival signals for an ensemble of single-particle events are averaged together, we see that prompt and delayed SOA particles have the same peak shape (Figure 8a). Here, we display the average single-particle mass signal for particles with the same arrival time. We chose two arrival-time bins with times-of-flight equal to 3.21 ms and 4.05 ms. All particles in each bin are categorized as "prompt" and "delayed," respectively. The similar, sharp peak shape suggests that delayed particles are truly delayed in starting their vaporization process, and not simply evaporating at a slower rate. Drewnick et al. (2015) present the vaporization "event length" quantity, which is the full width at half maximum (FWHM) of mass arrival signals from individual particles. In our study, the time resolution of the mass arrival trace (determined by the pulser period, 30 μs) is on the same order as the event length, which does not allow us to quantify the event length with any precision. However, qualitatively we can say that prompt and delayed particles for the SOA presented here have similar event lengths, and are on the order of $\sim$30 μs, similar to those measured by Drewnick et al. (2015) for ammonium sulfate aerosol. We found nearly identical event lengths for prompt versus delayed ammonium sulfate as well, indicating that ammonium sulfate exhibits the same behavior of "flash vaporizing" even when the particles are delayed. The event length for ammonium nitrate aerosol at low vaporizer temperatures, however, is fundamentally different (see Figure 8b); mass arrives over a much longer timescale (1 ms), indicating that particles are sticking to the vaporizer and slowly losing mass. Thus we conclude that delayed SOA, as well as ammonium sulfate, particles must be bouncing around the ionization cage after initially striking the front of the vaporizer before they finally land and flash-vaporize on one of the hot surfaces in the vaporization region (e.g. side of the vaporizer, ionization cage). Our conclusion is the same as that of Cross et al. (2009), who identified this mechanism acting on delayed particles in ambient measurements in Mexico City.

The AMS vaporizer is a cylindrical tube furnace (r = 3.81 mm; l = 20 mm) with a concave beveled cone (60° included angle) serving as the stop for the particle beam. It is centered within an ionization cage, a rectangular stainless steel housing (h = 6 mm; w = 8 mm; l = 15 mm) which is open on each end. The front end of the vaporizer is set back $\sim$10 mm from the front opening of the ion cage, and $\sim$2 mm from the ion extraction volume, maximizing the intersection of the vaporized particle plume,

Atmos. Meas. Tech. Discuss., doi:10.5194/amt-2016-271, 2016
Manuscript under review for journal Atmos. Meas. Tech.
Published: 12 September 2016

the electron beam from the filament, and the axis of ion extraction. Because of the long hot surface of the vaporizer, which is housed inside a sheet-metal cage, this mechanistic picture of particles bouncing around this region before finally landing on a hot surface is plausible. Importantly, for this SOA, the actual vaporization of the particle still can be thought of as rapid—when the particle finally does stick, it is vaporized and ionized on the same timescale as a "prompt" particle. Thus, the "PToF broadening" shown in Figure 2 can be attributed to SOA particles bouncing around before vaporizing, not slowly boiling off adsorbed material over time, as discussed in Salcedo et al. (2010) for lead salts (e.g. $PbCl^+$), and in Drewnick et al. (2015) for sea salt and other semi-refractory components (e.g. ZnI_2). Furthermore, this explanation is consistent with the decrease in IPP as a function of delay time: when particles vaporize on e.g. the side of the vaporizer, they are in a sub-optimal position for ionization of the resulting vapor plume and thus detection of the full single-particle mass (Huffman et al., 2009). From Figure 6, the decrease in IPP with delay times up to 1 ms indicate an increasingly sub-optimal average vaporization location for the particle with respect to the ionization region. For long delay times (>1 ms), the likelihood of the particle landing near the ionization region becomes very low, but further delay does not influence the effective ionization efficiency. As indicated by wide spread of IPP values for a given delay time in Figure 6, it is very unlikely that a long-delayed particle can provide as many ions to the mass detector that the average prompt particle can.

In Figure 6 we also show a secondary x axis of distance based on the nominal particle velocity. This is the distance traveled after the initial particle impact on the vaporizer, assuming elastic scattering as the particle bounces. The inferred distance is long compared to the length scales of the ionization region. We thus conclude that the particles are probably literally bouncing randomly around the ionization region, impelled by surfaces that are rough at the length scale of the particles. The top x-axis of Figure 6 shows our estimate for the nominal distance bounced for these 370 nm particles. For this calculation we used the average measured velocity of the prompt particles, as measured between the chopper and laser. Comparing the length scales (∼1 cm) of the ionization cage and vaporizer with our estimated distance bounced based on delay times, the most delayed particles are experiencing many collisions with ionizer/vaporizer surfaces before finally vaporizing.

As a further check that the SOA particles measured in LSSP mode are rapidly vaporizing—just simply doing so at a time later than would be expected based on their measured size and expected time-of-flight—we increased the temperature of the vaporizer from 600 °C to 800 °C. Were the particles sitting on the vaporizer surface and slowly boiling, we would expect this temperature increase to decrease the broadened PToF tail (Figure 9a). We do not see this effect (note: the degradation in the organic PToF signal at 800 °C is due to low particle numbers at the end of our experiment due to wall loss). However, when we coated SOA particles with squalane, a liquid at STP and a material that exhibits essentially no particle bounce in the AMS ($CE_p \sim 1$), and the broadened tail of the SOA mass distribution diminished. When we heated the chamber, causing the squalane to evaporate, the

Atmos. Meas. Tech. Discuss., doi:10.5194/amt-2016-271, 2016
Manuscript under review for journal Atmos. Meas. Tech.
Published: 12 September 2016

Atmospheric Measurement Techniques Discussions

broadened tail reappeared. This further supports this idea that delayed SOA particles are bouncing around the vaporizer-ionizer region before finally flash-vaporizing (Figure 9b).

On the other hand, the PToF distribution for ammonium nitrate can be broadened by decreasing the vaporizer temperature from 600 °C to 200 °C. Figure 9b shows the mass distribution of *m/z* 46 (NO_2^+) for both vaporizer temperatures. The increase in PToF arrival times (which translates to the broadened mass distribution) with decreased vaporizer temperature indicates that these particles do stick to the surface, and have a reduced mass flux at lower temperatures, thus spreading the signal arrival out over time-of-flight (Figure 9b). Docherty et al. (2015), operating their vaporizer temperature on a programmed cycle between 200 and 600 °C, also see PToF broadening for nitrate in ambient data. Mass arrival signals from individual ammonium nitrate particles at these low vaporizer temperatures are much longer (event lengths ∼200 μs, consistent with those measured by Drewnick et al., 2015) than those shown for prompt and delayed SOA particles in Figure 8. There seem to be different mechanisms for particle delay both for different operating conditions of the AMS and for different particle types.

Consistent with this proposed mechanism—that delayed SOA particles are bouncing around and vaporizing on surfaces away from the vaporizer cone—there are differences in mass spectra between prompt and delayed particles. Figure 10 shows the difference mass spectrum between prompt and delayed particles for both SOA and ammonium sulfate, both of which exhibit a high delayed fraction. We created average mass spectra for prompt and delayed particles by summing the single-particle spectra for each category and dividing by the number of particles. We then normalized these average spectra by the sum of ions across all *m/z*, and the difference mass spectra is the normalized prompt MS minus normalized delayed MS. Error bars indicate the propagated standard error of the mean at each *m/z*.

Several fragments are more prominent in either the prompt or delayed mass spectra, colored by blue and red sticks, respectively. For instance, *m*/z 43 (mostly $C_2H_3O^+$) is higher and *m*/z 44 (CO_2^+) is lower for delayed SOA particles; the acidic fragments *m*/z 81 (HSO_3^+) and 98 ($H_2SO_4^+$) are higher in the delayed MS for ammonium sulfate particles while *m*/z 48 (SO^+) and 64 (SO_2^+) are higher in the prompt MS for ammonium sulfate. The ammonium ion (NH_4^+) is enhanced in the prompt MS, while ammonia (NH_3^+) is enhanced in the delayed MS for ammonium sulfate particles. We attribute these differences in mass spectra between prompt and delayed particles to the wide range of possible temperatures experieneced by delayed particles that have bounced away from the center of the AMS vaporizer. The lower temperatures at these sub-optimal vaporization positions (e.g. side of the vaporizer, on the ion cage, etc.) can lead to different fragmentation pathways, which could be important for interpreting ambient single-particle spectra.

To support this hypothesis, we look at previous work conducted by Docherty et al. (2015). They show that acidic fragments from ambient ammonium sulfate measured during the Study of Organic Aerosols at Riverside (SOAR-2005) are enhanced when they lower the AMS vaporizer temperature

Atmos. Meas. Tech. Discuss., doi:10.5194/amt-2016-271, 2016
Manuscript under review for journal Atmos. Meas. Tech.
Published: 12 September 2016

from 600 °C to 200 °C, which is consistent with our hypothesis that delayed ammonium sulfate particles were vaporizing on cooler surfaces. Docherty et al. (2015) also show that ambient OA in SOAR-2005 appeared more oxidized at lower vaporizer temperatures, as indicated by increased f_{44} and increased O:C. While f_{44} is slightly higher in our prompt SOA MS, perhaps indicating that the prompt particles appear more oxidized, the rest of the mass spectrum shows that the delayed particles are enhanced in oxidized fragments, while the prompt particles are enhanced in reduced fragments. We see an enhancement in the delayed MS of C_xH_yO fragments, such *m*/z 71 ($C_4H_7O^+$), *m*/z 83 ($C_5H_7O^+$), and *m*/z 97 ($C_6H_9O^+$). Other studies have found that f_{44} does not change or even decreases with lower vaporizer temperatures compared to the standard 600 °C; for example, Canagaratna et al. (2015) showed that f_{44} decreases in the MS of cis-pinonic acid at 200 °C compared to the standard temperature. Thus, the enhancement of these $C_xH_yO^+$ fragments in the delayed MS is a more robust indicator than f_{44} that our delayed SOA particles appear more oxidized than the prompt ones. Excluding f_{44}, our data are consistent with Docherty et al. (2015) and the hypothesis that our delayed particles are bouncing around the vaporization/ionization region before landing on cooler surfaces and finally evaporating. Importantly, these data show that particles delayed due to particle bounce, like ammonium sulfate and the SOA studied here, can have differences in their mass spectra that need to be considered when analyzing ambient single-particle data.

3.5 Collection efficiency as a function of size and thermodenuder temperature

As reported previously in the literature, some studies have shown collection efficiency for OA to be size (Liu et al. (2013)) and composition-dependent (Docherty et al., 2013). To investigate any size-dependent collection efficiency that our SOA might have, we selected particles at different mobility diameters with a DMA upstream of the AMS. Figure 11a shows CE_p as a function of selected mobility diameter. LSSP can also provide a size-resolved CE_p for polydisperse aerosol (as in Liu et al., 2013), as each optically-counted particle has an estimated d_{va}. Figure 11a also shows CE_p for polydisperse SOA from multiple smog-chamber experiments, which agree well with the size-selected data. The CE_p for SOA studied here was not a strong function of size between in diameter range 170-460 nm. The mean CE_p across all experiments for SOA was 0.3 ($\pm$0.04 S.D.), and ranged from as low as 0.25 to as high as 0.4.

While CE_p for this SOA is independent of size, we do observe a decreasing trend in CE_p by passing the SOA through a thermodenuder. We sampled SOA alternately through a thermally-denuded line, or through a bypass line of the same length held at the same temperature as the chamber. Figure 11 shows CE_p plotted against thermodenuder temperature for an experiment where SOA particles passed through a thermal denuder operating on a temperature ramp profile. The ramp program increased temperature linearly over one hour from 27 °C to 130 °C, soaked at 130 °C for 10 minutes, and then returned back to 27 °C at the same rate. Above 110 °C, almost all SOA evaporated in the thermodenuder, making the CE_p measurement impossible. The CE_p values in Figure 11 are calcu-

Atmos. Meas. Tech. Discuss., doi:10.5194/amt-2016-271, 2016
Manuscript under review for journal Atmos. Meas. Tech.
Published: 12 September 2016

lated for particles with 200 nm > d_{va} >300nm to isolate the effects of volatility and/or oxidation state on CE_p, instead of measuring smaller particles less likely to provide enough detectable mass above the threshold.

We use temperature as a proxy variable for the volatility of the aerosol, because SOA particles that have passed through the denuder will have had some fraction of their more-volatile components removed, the amount of which increases with increasing temperature. We color data points in Figure 11 by f_{44} as measured from MS mode bulk mass spectra, which is used in AMS analysis as both a direct measurement of oxidation state and a proxy for OA volatility (Ng et al., 2011). These data show that CE_p is inversely related to either the SOA oxidation state, volatility, or both. These results are consistent with the trend shown by Docherty et al. (2013), who saw decreasing CE_m with increasing oxidation state, though are within the range of scatter shown in Figure 11a for all SOA experiments. It should be noted that this SOA is similarly oxidized ($f_{44}/f_{57} \approx 6$) as the least oxidized SOA from their study ($f_{44}/f_{57} \geq 5$), which had a CE_m of ~0.2 ($f_{44}/f_{57} \geq 5$). SOA sampled through the bypass line during this same time period did not have any decrease in CE_p. It is not possible to determine whether the decrease in CE_p is attributable to changes in volatility or oxidation state, as the two are coupled in our measurements. However, this example shows that LSSP can be used to verify whether this trend in CE_p with these compositional changes exists for other types of NR-PM_1.

4 Conclusions

In this study, we present LSSP AMS data that gives further insights into the nature of collection efficiency for the common laboratory system of SOA from α pinene + O_3. SOA generated in these experiments exhibited an artificial tail in the PToF distribution at large diameters, which we show to be an artifact of delayed vaporization. However, by studying the arrival of mass signals for these delayed SOA particles, we see that the signals can not be attributed to adsorption on the AMS vaporizer followed by slow evaporation. Rather, particles bounce off the vaporizer after primary impact and vaporize on some subsequent impact with a hot surface in the vaporization region. This causes the mass arrival at the detector to be delayed relative to the estimated speed from optical detection, but is fundamentally different than slow evaporation from the vaporizer surface. A significant fraction of SOA and ammonium sulfate exhibited this type of delayed vaporization, while ammonium nitrate and squalane exhibited none. For delayed particles, the measured per-particle mass signal is reduced, which we report as ions per particle as a function of delay time. The artificially broadened PToF distributions would be even more prominent if the delayed particles had the same effective ionization efficiency as prompt particles. However, some of the SOA particles counted as null evidently evaporate on very long timescales relative to the chopper cycle, as indicated by CE_m >CE_p. These particles register no mass signal in LSSP mode, and are labeled as "null," though what fraction of null particles will result in detectable mass on the long timescale of MS mode is not discernible using

Atmos. Meas. Tech. Discuss., doi:10.5194/amt-2016-271, 2016
Manuscript under review for journal Atmos. Meas. Tech.
Published: 12 September 2016

these data. The reduced number of ions per particle of delayed particles means that the AMS PToF signal for polydisperse distributions will be dominated by prompt particles, because larger prompt particles with high IPP will overwhelm smaller delayed particles with lower mass and few ions per unit mass. However, the large diameter tail in the AMS PToF spectrum should be regarded with caution. Additionally, we use the LSSP to show that particle collection efficiency is not a function of size for the size range explored ($170 < d_m < 460$ nm), but is related to the oxidation state/volatility of this SOA.

Rather than being viewed as a limitation, collection efficiency should be viewed as a sensitivity within the AMS that simply needs to be understood for a given system and that may provide additional useful information. We demonstrate here that using the LSSP capabilities of the AMS allows users to gain further insight into a given aerosol system. Further work should be conducted to better understand any compositional artifacts that may be attributable to delayed vaporization. Data of this kind may also possibly be used for design improvements to the vaporization region.

Acknowledgements. This research was supported by grant CHE1412309 from the National Science Foundation. The High-Resolution Aerosol Mass Spectrometer was purchased with Major Research Instrumentation funds from grant CBET0922643 through the National Science Foundation, and generous support of the Wallace Research Foundation. The authors would like to thank Rawad Saleh, Manjula Canagaratna, John Jayne, and Eben Cross for useful discussions regarding data analysis. Thanks for John-Charles Baucom for his help with the design and construction of the vaporizer used to prepare squalane aerosol.

Atmos. Meas. Tech. Discuss., doi:10.5194/amt-2016-271, 2016
Manuscript under review for journal Atmos. Meas. Tech.
Published: 12 September 2016

Atmospheric Measurement Techniques Discussions

References

Aiken, A. C., DeCarlo, P. F., Kroll, J. H., Worsnop, D. R., Huffman, J. A., Docherty, K. S., Ulbrich, I. M., Mohr, C., Kimmel, J. R., Sueper, D., Sun, Y., Zhang, Q., Trimborn, A., Northway, M., Ziemann, P. J., Canagaratna, M. R., Onasch, T. B., Alfarra, M. R., Prevot, A. S. H., Dommen, J., Duplissy, J., Metzger, A., Baltensperger, U., and Jimenez, J. L.: O/C and OM/OC Ratios of Primary, Secondary, and Ambient Organic Aerosols with High-Resolution Time-of-Flight Aerosol Mass Spectrometry, Environmental Science & Technology, 42, 4478–4485, 2008.

Alfarra, M. R.: Insights Into Atmospheric Organic Aerosols Using an Aerosol Mass Spectrometer, Ph.D. thesis, University of Manchester, 2004.

Bahreini, R., Keywood, M. D., Ng, N. L., Varutbangkul, V., Gao, S., Flagan, R. C., Seinfeld, J. H., Worsnop, D. R., and Jimenez, J. L.: Measurements of Secondary Organic Aerosol from Oxidation of Cycloalkenes, Terpenes, and m-Xylene Using an Aerodyne Aerosol Mass Spectrometer, Environmental Science & Technology, 39, 5674–5688, 2005.

Canagaratna, M. R., Jayne, J., Jimenez, J. L., Allan, J. D., Alfarra, M. R., Zhang, Q., Onasch, T. B., Drewnick, F., Coe, H., middlebrook, A., Delia, A., Williams, L. R., Trimborn, A. M., Northway, M. J., DeCarlo, P. F., Kolb, C., davidovits, P., and Worsnop, D. R.: Chemical and microphysical characterization of ambient aerosols with the aerodyne aerosol mass spectrometer, Mass Spectrometry Reviews, 26, 185–222, 2007.

Canagaratna, M. R., Jimenez, J. L., Kroll, J. H., Chen, Q., Kessler, S. H., Massoli, P., Hildebrandt Ruiz, L., Fortner, E., Williams, L. R., Wilson, K. R., Surratt, J. D., Donahue, N. M., Jayne, J., and Worsnop, D. R.: Elemental ratio measurements of organic compounds using aerosol mass spectrometry: characterization, improved calibration, and implications, Atmospheric Chemistry and Physics, 15, 253–272, 2015.

Craven, J. S., Yee, L. D., Ng, N. L., Canagaratna, M. R., Loza, C. L., Schilling, K. A., Yatavelli, R. L. N., Thornton, J. A., Ziemann, P. J., Flagan, R. C., and Seinfeld, J. H.: Analysis of secondary organic aerosol formation and aging using positive matrix factorization of high-resolution aerosol mass spectra: application to the dodecane low-$NO_{xsystem}$, Atmospheric Chemistry and Physics, 12, 11 795–11 817, 2012.

Cross, E., Onasch, T., Canagaratna, M., Jayne, J., Kimmel, J., Yu, X., Alexander, M., Worsnop, D., and davidovits, P.: Single particle characterization using a light scattering module coupled to a time-of-flight aerosol mass spectrometer, Atmospheric Chemistry and Physics, 9, 7769–7793, 2009.

Cross, E. S., Slowik, J. G., Davidovits, P., Allan, J. D., Worsnop, D. R., Jayne, J. T., Lewis, D. K., Canagaratna, M., and Onasch, T. B.: Laboratory and Ambient Particle Density Determinations using Light Scattering in Conjunction with Aerosol Mass Spectrometry, Aerosol Science and Technology, 41, 343–359, 2007.

DeCarlo, P. F., Slowik, J. G., Worsnop, D. R., Davidovits, P., and Jimenez, J. L.: Particle Morphology and Density Characterization by Combined Mobility and Aerodynamic Diameter Measurements. Part 1: Theory, Aerosol Science and Technology, 38, 1185–1205, 2004.

DeCarlo, P. F., Kimmel, J. R., Trimborn, A., Northway, M. J., Jayne, J. T., Aiken, A. C., Gonin, M., Fuhrer, K., Horvath, T., Docherty, K. S., Worsnop, D. R., and Jimenez, J. L.: Field-Deployable, High-Resolution, Time-of-Flight Aerosol Mass Spectrometer, Analytical Chemistry, 78, 8281–8289, 2006.

Docherty, K. S., Jaoui, M., Corse, E., Jimenez, J. L., Offenberg, J. H., Lewandowski, M., and Kleindienst, T. E.: Collection Efficiency of the Aerosol Mass Spectrometer for Chamber-Generated Secondary Organic Aerosols, Aerosol Science and Technology, 47, 294–309, 2013.

Atmos. Meas. Tech. Discuss., doi:10.5194/amt-2016-271, 2016
Manuscript under review for journal Atmos. Meas. Tech.
Published: 12 September 2016

Atmospheric Measurement Techniques Discussions

Docherty, K. S., Lewandowski, M., and Jimenez, J. L.: Effect of Vaporizer Temperature on Ambient Non-Refractory Submicron Aerosol Composition and Mass Spectra Measured by the Aerosol Mass Spectrometer, Aerosol Science and . . . , 2015.

Drewnick, F., Schwab, J. J., Hogrefe, O., Peters, S., Husain, L., Diamond, D., Weber, R., and Demerjian, K. L.: Intercomparison and evaluation of four semi-continuous PM2.5 sulfate instruments, Atmospheric Environment, 37, 3335–3350, 2003.

Drewnick, F., Hings, S. S., DeCarlo, P., Jayne, J. T., Gonin, M., Fuhrer, K., Weimer, S., Jimenez, J. L., Demerjian, K. L., Borrmann, S., and Worsnop, D. R.: A New Time-of-Flight Aerosol Mass Spectrometer (TOF-AMS)—Instrument Description and First Field Deployment, Aerosol Science and Technology, 39, 637–658, 2005.

Drewnick, F., Diesch, J. M., Faber, P., and Borrmann, S.: Aerosol mass spectrometry: particle–vaporizer interactions and their consequences for the measurements, Atmospheric Measurement Techniques, 8, 3811–3830, 2015.

Huffman, J. A., Jayne, J. T., Drewnick, F., Aiken, A. C., Onasch, T., Worsnop, D. R., and Jimenez, J. L.: Design, Modeling, Optimization, and Experimental Tests of a Particle Beam Width Probe for the Aerodyne Aerosol Mass Spectrometer, Aerosol Science and Technology, 39, 1143–1163, 2005.

Huffman, J. A., Docherty, K. S., Aiken, A. C., Cubison, M. J., Ulbrich, I. M., DeCarlo, P. F., Sueper, D., Jayne, J., Worsnop, D. R., and Ziemann, P. J.: Chemically-resolved aerosol volatility measurements from two megacity field studies, Atmospheric Chemistry and Physics, 9, 7161–7182, 2009.

Jimenez, J. L., Jayne, J. T., Shi, Q., Kolb, C. E., Worsnop, D. R., Yourshaw, I., Seinfeld, J. H., Flagan, R. C., Zhang, X., and Smith, K. A.: Ambient aerosol sampling using the aerodyne aerosol mass spectrometer, Journal of Geophysical Research: Atmospheres (1984–2012), 108, 2003.

Jimenez, J. L., Canagaratna, M. R., Donahue, N. M., Prevot, A. S. H., Zhang, Q., Kroll, J. H., DeCarlo, P. F., Allan, J. D., Coe, H., Ng, N. L., Aiken, A. C., Docherty, K. S., Ulbrich, I. M., Grieshop, A. P., Robinson, A. L., Duplissy, J., Smith, J. D., Wilson, K. R., Lanz, V. A., Hueglin, C., Sun, Y. L., Tian, J., Laaksonen, A., Raatikainen, T., Rautiainen, J., Vaattovaara, P., Ehn, M., Kulmala, M., Tomlinson, J. M., Collins, D. R., Cubison, M. J., E., Dunlea, J., Huffman, J. A., Onasch, T. B., Alfarra, M. R., Williams, P. I., Bower, K., Kondo, Y., Schneider, J., Drewnick, F., Borrmann, S., Weimer, S., Demerjian, K., Salcedo, D., Cottrell, L., Griffin, R., Takami, A., Miyoshi, T., Hatakeyama, S., Shimono, A., Sun, J. Y., Zhang, Y. M., Dzepina, K., Kimmel, J. R., Sueper, D., Jayne, J., Herndon, S. C., Trimborn, A. M., Williams, L. R., Wood, E. C., Middlebrook, A. M., Kolb, C., Baltensperger, U., and Worsnop, D. R.: Evolution of Organic Aerosols in the Atmosphere, Science, 326, 1525–1529, 2009.

Kanakidou, M., Seinfeld, J. H., Pandis, S. N., Barnes, I., Dentener, F. J., Facchini, M. C., Van Dingenen, R., Ervens, B., Nenes, A., and Nielsen, C. J.: Organic aerosol and global climate modelling: a review, Atmospheric Chemistry and Physics, 5, 1053–1123, 2005.

Kostenidou, E., Pathak, R. K., and Pandis, S. N.: An Algorithm for the Calculation of Secondary Organic Aerosol Density Combining AMS and SMPS Data, Aerosol Science and Technology, 41, 1002–1010, 2007.

Lightstone, J. M., Onasch, T. B., Imre, D., and Oatis, S.: Deliquescence, Efflorescence, and Water Activity in Ammonium Nitrate and Mixed Ammonium Nitrate/Succinic Acid Microparticles, The Journal of Physical Chemistry A, 104, 9337–9346, 2000.

Atmos. Meas. Tech. Discuss., doi:10.5194/amt-2016-271, 2016
Manuscript under review for journal Atmos. Meas. Tech.
Published: 12 September 2016

Atmospheric Measurement Techniques Discussions

Liu, S., Russell, L. M., Sueper, D. T., and Onasch, T. B.: Organic particle types by single-particle measurements using a time-of-flight aerosol mass spectrometer coupled with a light scattering module, Atmospheric Measurement Techniques, 6, 187–197, 2013.

Lozano, R., Naghavi, M., Foreman, K., Lim, S., Shibuya, K., Aboyans, V., Abraham, J., Adair, T., Aggarwal, R., and Ahn, S. Y.: Global and regional mortality from 235 causes of death for 20 age groups in 1990 and 2010: a systematic analysis for the Global Burden of Disease Study 2010, The Lancet, 380, 2095–2128, 2013.

Matthew, B. M., Middlebrook, A. M., and Onasch, T. B.: Collection efficiencies in an Aerodyne Aerosol Mass Spectrometer as a function of particle phase for laboratory generated aerosols, Aerosol Science and Technology, 42, 884–898, 2008.

Mensah, A. A., Buchholz, A., Mentel, T. F., Tillmann, R., and Kiendler-Scharr, A.: Journal of Aerosol Science, Journal of Aerosol Science, 42, 11–19, 2011.

Middlebrook, A. M., Bahreini, R., Jimenez, J. L., and Canagaratna, M. R.: Evaluation of Composition-Dependent Collection Efficiencies for the Aerodyne Aerosol Mass Spectrometer using Field Data, Aerosol Science and Technology, 46, 258–271, 2012.

Murphy, D. M.: The effects of molecular weight and thermal decomposition on the sensitivity of a thermal desorption aerosol mass spectrometer, Aerosol Science and Technology, 50, 118–125, 2015.

Myers, R. L. and Fite, W. L.: Electrical detection of airborne particulates using surface ionization techniques, Environmental Science & Technology, 9, 334–336, 1975.

Ng, N. L., Canagaratna, M. R., Jimenez, J. L., Chhabra, P. S., Seinfeld, J. H., and Worsnop, D. R.: Changes in organic aerosol composition with aging inferred from aerosol mass spectra, Atmospheric Chemistry and Physics, 11, 6465–6474, 2011.

Pankow, J. and Asher, W.: SIMPOL. 1: a simple group contribution method for predicting vapor pressures and enthalpies of vaporization of multifunctional organic compounds, Atmospheric Chemistry and Physics, 8, 2773–2796, 2008.

Quinn, P. K., Bates, T. S., Coffman, D., Onasch, T. B., Worsnop, D., Baynard, T., de Gouw, J. A., Goldan, P. D., Kuster, W. C., Williams, E., Roberts, J. M., Lerner, B., Stohl, A., Pettersson, A., and Lovejoy, E. R.: Impacts of sources and aging on submicrometer aerosol properties in the marine boundary layer across the Gulf of Maine, Journal of Geophysical Research, 111, D23S36, 2006.

Richardson, C. B. and Hightower, R. L.: Evaporation of ammonium nitrate particles, Atmospheric Environment (1967), 21, 971–975, 1987.

Robinson, E. S., Saleh, R., and Donahue, N. M.: Organic Aerosol Mixing Observed by Single-Particle Mass Spectrometry, The Journal of Physical Chemistry A, 117, 13 935–13 945, 2013.

Robinson, E. S., Saleh, R., and Donahue, N. M.: Probing the Evaporation Dynamics of Mixed SOA/Squalane Particles Using Size-Resolved Composition and Single-Particle Measurements, Environmental Science & Technology, 49, 9724–9732, 2015.

Salcedo, D., Onasch, T. B., Canagaratna, M. R., Dzepina, K., Huffman, J. A., Jayne, J., Worsnop, D. R., Kolb, C., Weimer, S., and Drewnick, F.: Technical Note: Use of a beam width probe in an Aerosol Mass Spectrometer to monitor particle collection efficiency in the field, Atmospheric Chemistry and Physics, 7, 549–556, 2007.

Atmos. Meas. Tech. Discuss., doi:10.5194/amt-2016-271, 2016
Manuscript under review for journal Atmos. Meas. Tech.
Published: 12 September 2016

Salcedo, D., Onasch, T. B., Aiken, A. C., Williams, L. R., de Foy, B., Cubison, M. J., Worsnop, D. R., Molina, L. T., and Jimenez, J. L.: Determination of particulate lead using aerosol mass spectrometry: MILAGRO/MCMA-2006 observations, Atmospheric Chemistry and Physics, 10, 5371–5389, 2010.

Saleh, R., Robinson, E. S., Ahern, A. A., and Donahue, N. M.: Evaporation rate of particles in the vaporizer of the Aerodyne Aerosol Mass Spectrometer, Aerosol Science and Technology, in preparation, 2016.

Shilling, J. E., Chen, Q., King, S. M., Rosenoern, T., Kroll, J. H., Worsnop, D. R., DeCarlo, P. F., Aiken, A. C., Sueper, D., and Jimenez, J. L.: Loading-dependent elemental composition of α-pinene SOA particles, Atmospheric Chemistry and Physics, 9, 771–782, 2009.

Silva, P. J., Erupe, M. E., Price, D., Elias, J., G J Malloy, Q., Li, Q., Warren, B., and Cocker, D. R.: Trimethylamine as Precursor to Secondary Organic Aerosol Formation via Nitrate Radical Reaction in the Atmosphere, Environmental Science & Technology, 42, 4689–4696, 2008.

Slowik, J. G., Stroud, C., Bottenheim, J. W., Brickell, P. C., Chang, R.-W., Liggio, J., Makar, P. A., Martin, R. V., Moran, M. D., and Shantz, N. C.: Characterization of a large biogenic secondary organic aerosol event from eastern Canadian forests, Atmospheric Chemistry and Physics Discussions, 9, 18 113–18 158, 2009.

Solomon, S., Qin, D., Manning, M., Alley, R. B., Berntsen, T., Bindoff, N. L., Chen, Z., Chidthaisong, A., Gregory, J. M., and Hegerl, G. C.: Climate change 2007: The physical science basis, contribution of working group 1 to the fourth assessment report of the Intergovernmental Panel on Climate Change, 2007.

Virtanen, A., Joutsensaari, J., Koop, T., Kannosto, J., Yli-Pirilä, P., Leskinen, J., Mäkelä, J. M., Holopainen, J. K., Pöschl, U., Kulmala, M., Worsnop, D. R., and Laaksonen, A.: An amorphous solid state of biogenic secondary organic aerosol particles, Nature, 467, 824–827, 2010.

Zelenyuk, A., Yang, J., Song, C., Zaveri, R. A., and Imre, D.: A New Real-Time Method for Determining Particles' Sphericity and Density: Application to Secondary Organic Aerosol Formed by Ozonolysis of α-Pinene, Environmental Science & Technology, 42, 8033–8038, 2008.

Atmos. Meas. Tech. Discuss., doi:10.5194/amt-2016-271, 2016
Manuscript under review for journal Atmos. Meas. Tech.
Published: 12 September 2016

Atmospheric Measurement Techniques Discussions

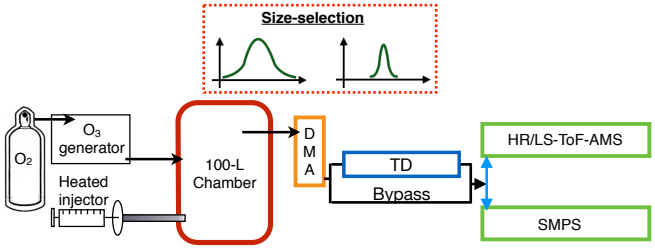

Fig. 1: Experimental setup for SOA CE experiments.

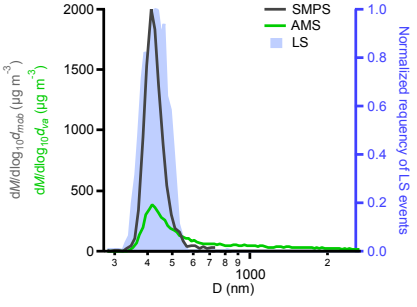

Fig. 2: Ensemble mass distributions from SMPS (black trace, adjusted for density) and AMS (green trace) of size-selected α-pinene derived SOA particles with 370 nm mobility diameter for an example SOA experiment. Frequency of optically-counted particles (from LSSP) as a function of size shown in blue. For this instance, CE_m = 0.39. The blue trace is normalized to 1 and plotted on the right axis as to have the same height as the SMPS trace, reflecting that optical detection in the AMS flight chamber is not affected by particle bounce.

Atmos. Meas. Tech. Discuss., doi:10.5194/amt-2016-271, 2016
Manuscript under review for journal Atmos. Meas. Tech.
Published: 12 September 2016

Atmospheric Measurement Techniques Discussions

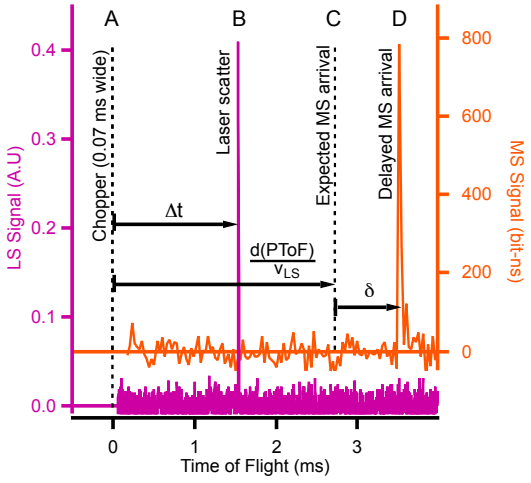

Fig. 3: Scattered light signal (magenta) and mass spectrometer signal (orange) as a function of particle time-of-flightfor an example delayed particle. The particle velocity (v_{LS}) is calculated by the measured time between the start of the chopper cycle (point "A") and detection of the scattered light peak (B). The velocity is used to estimate an expected arrival time of the chemical ion signal at the mass spectrometer (C) assuming prompt evaporation and ionization of the particle at the vaporizer. The difference between the expected (C) and actual (D) arrival times is denoted by δ, and allows for the operational definition of prompt and delayed particle events.

Atmos. Meas. Tech. Discuss., doi:10.5194/amt-2016-271, 2016
Manuscript under review for journal Atmos. Meas. Tech.
Published: 12 September 2016

Atmospheric Measurement Techniques Discussions

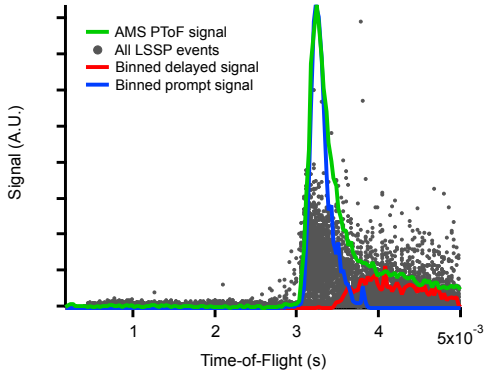

Fig. 4: Particle signal versus particle time-of-flight from the chopper to the mass detector are shown for ensemble mode (green trace) and for all detected single particle events (gray circles) in a representative SOA experiment (DMA size-selecting SOA particles with mobility diameter = 370 nm). Particles are sorted into either prompt or delayed categories based on their delay time. The mass signals for individual particles within each category are binned by flight time and summed to create the prompt (blue trace) and delayed (red trace) distributions.

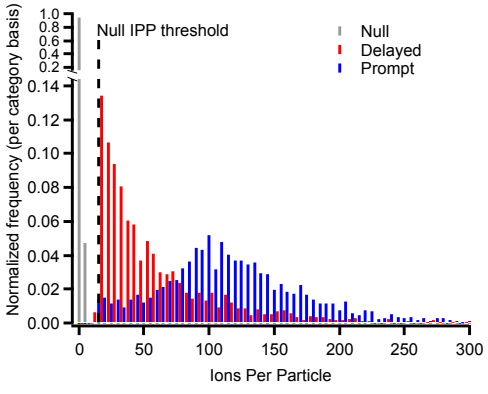

Fig. 5: Histogram of ions per particle for null (gray), delayed (red), and prompt (blue) particle categories for 370 nm SOA particles. The y-axis is the frequency of single-particle events within each category (in other words, all data for each category sum to one). The histogram bars for the delayed category are offset (by 5 ions) on the x-axis for clarity.

Atmos. Meas. Tech. Discuss., doi:10.5194/amt-2016-271, 2016
Manuscript under review for journal Atmos. Meas. Tech.
Published: 12 September 2016

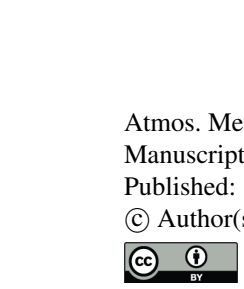

Atmospheric Measurement Techniques Discussions

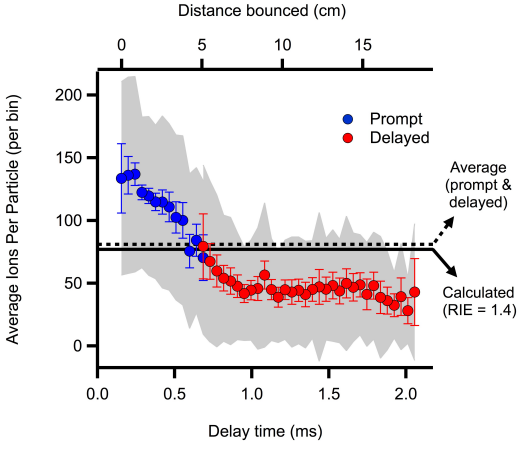

Fig. 6: Ions per particle as a function of the delay time between the expected time of arrival for the chemical ion signal and the actual time of arrival for 370 nm SOA particles. The data points are the arithmetic mean IPP value for a given delay time bin. Error bars are the standard error of the mean for each bin, which represent the precision of the average IPP values. The gray shadow behind is the standard deviation of ions per particle within each bin, which reflects the inherent spread of single particle signals at a given delay time for monodisperse SOA. Dotted line shows the average IPP for the entire ensemble, while the solid line shows the calculated IPP based on an ionization efficiency (IE) of 5e-7 and an RIE of 1.4 for organics compared to ammonium nitrate. We also estimate the nominal distance bounced (top x-axis) for these particles, assuming the average velocity of the size-selected particles measured between the chopper and laser.

Atmos. Meas. Tech. Discuss., doi:10.5194/amt-2016-271, 2016
Manuscript under review for journal Atmos. Meas. Tech.
Published: 12 September 2016

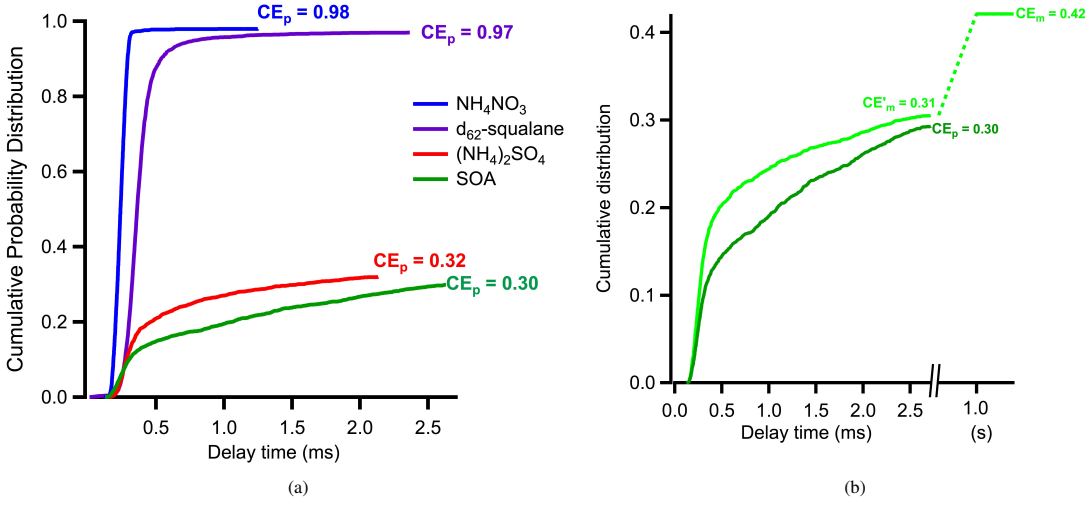

Fig. 7: (a) Cumulative probability distributions of particle counts as a function of delay time for ammonium nitrate (blue), D_{62}-squalane (purple), ammonium sulfate (red), and SOA (green). All traces are normalized by the respective CE_p values, which is the average value across all experiments for that particle type. (b) Cumulative probability distributions for single particle counts (dark green) and single-particle mass (light green) for an individual SOA experiment. The dark green trace is scaled by CE_p. The light green trace, up to 2.5 ms delay time, is scaled by the mass collection efficiency as determined by comparing the AMS PToF-determined mass to the SMPS mass, according to equation 1. The broken axis represents additional mass seen beyond the window of the chopper cycle, and that mass is scaled according to the mass collection efficiency determined by the AMS mass seen in MS mode compared to the SMPS mass.

Atmos. Meas. Tech. Discuss., doi:10.5194/amt-2016-271, 2016
Manuscript under review for journal Atmos. Meas. Tech.
Published: 12 September 2016

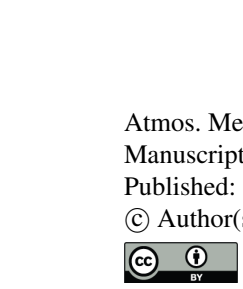

Atmospheric Measurement Techniques Discussions

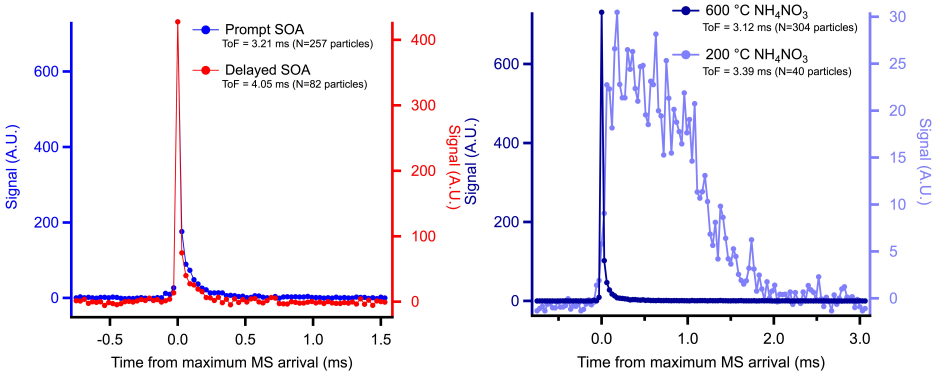

(a) (b)

Fig. 8: Profiles of single-particle mass arrival for SOA (a) and ammonium nitrate particles (b) under different vaporization scenarios. (a) Plot shows total chemical ion detection as a function of time from arrival of maximum signal for SOA. The traces represent the average signal for all particles with the same MS arrival time. The two arrival time bins shown correspond to either all prompt (ToF bin = 3.21 ms, blue trace) or delayed (ToF bin = 4.05 ms, red trace) particles. N is the number of particles used to make the average trace. (b) Similarly, average chemical signals as a function of arrival time are shown for ammonium nitrate particles at two different vaporizer temperatures. The arrival of mass at the detector (event length) is significantly longer for ammonium nitrate at 200 °C compared to 600 °C

Atmos. Meas. Tech. Discuss., doi:10.5194/amt-2016-271, 2016
Manuscript under review for journal Atmos. Meas. Tech.
Published: 12 September 2016

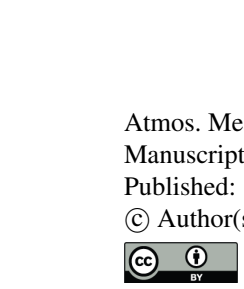

Atmospheric Measurement Techniques Discussions

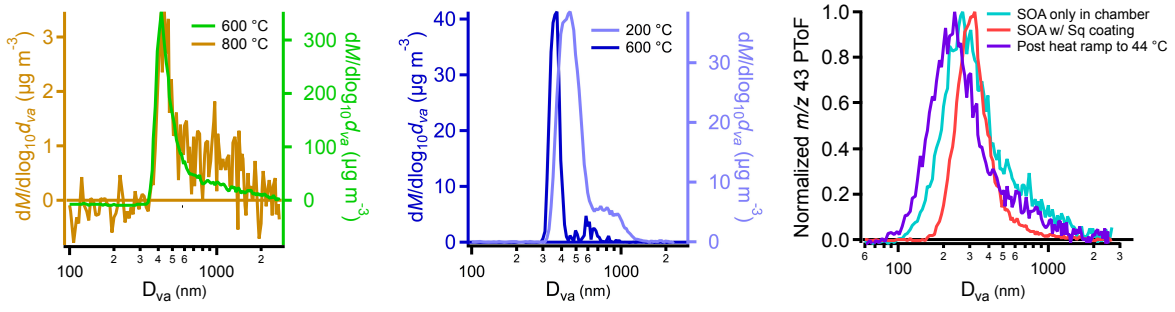

Fig. 9: Ensemble mass distributions of different particle types. (a) Organic mass distributions for α-pinene derived SOA particles at two different vaporizer temperatures with DMA-selected mobility diameter of 370 nm: 600 °C (green) and 800 °C (brown). Note: the degraded signal at 800 °C is due to low-particle numbers due to wall-loss, as these data were taken at the end of an experiment where particle number was relatively low. (b) *m/z* 46 PToF mass distributions for DMA-selected mobility diameter of 300 nm at the standard vaporizer temperature (600 °C, dark blue), and low temperature (200 °C, sky blue). (c) *m/z* 43 mass distributions from SOA particles at three stages of a mixed-particle experiment: homogeneously-nucleated SOA (teal), SOA particles coated with squalane (red), and SOA/squalane particles after an increase in chamber temperature (purple). Note the disappearance of the delayed tail with the condensation of squalane, and the reappearance of the tail with heating despite the decrease in mode diameter.

Atmos. Meas. Tech. Discuss., doi:10.5194/amt-2016-271, 2016
Manuscript under review for journal Atmos. Meas. Tech.
Published: 12 September 2016

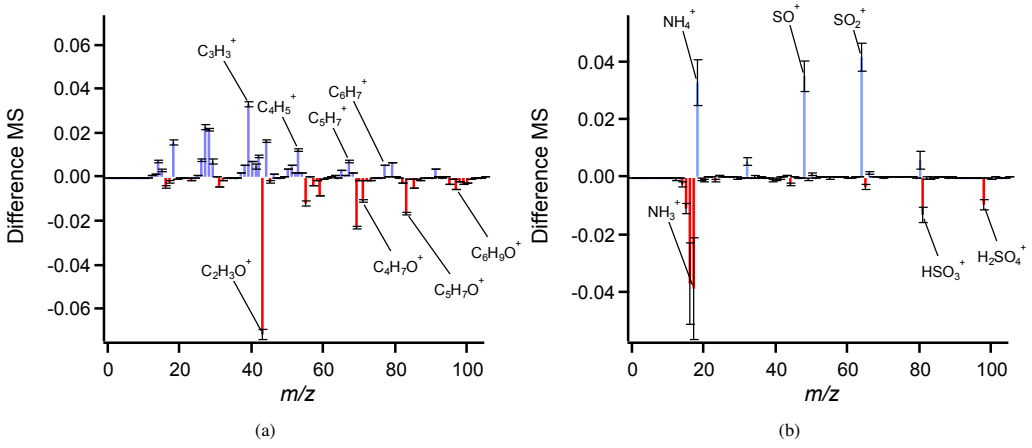

Fig. 10: Difference plots between prompt and delayed average mass spectra for (a) SOA and (B) ammonium sulfate. Plot is prepared by first normalizing each spectra by the total signal, and then subtracting the normalized delayed MS from the normalized prompt MS. Thus, mass fragments with positive values (blue) are enriched in the prompt MS, and those with negative values (red) are enriched in the delayed MS. Error bars are the propagated standard errors of the mean for each population.

Atmos. Meas. Tech. Discuss., doi:10.5194/amt-2016-271, 2016
Manuscript under review for journal Atmos. Meas. Tech.
Published: 12 September 2016

Atmospheric Measurement Techniques Discussions

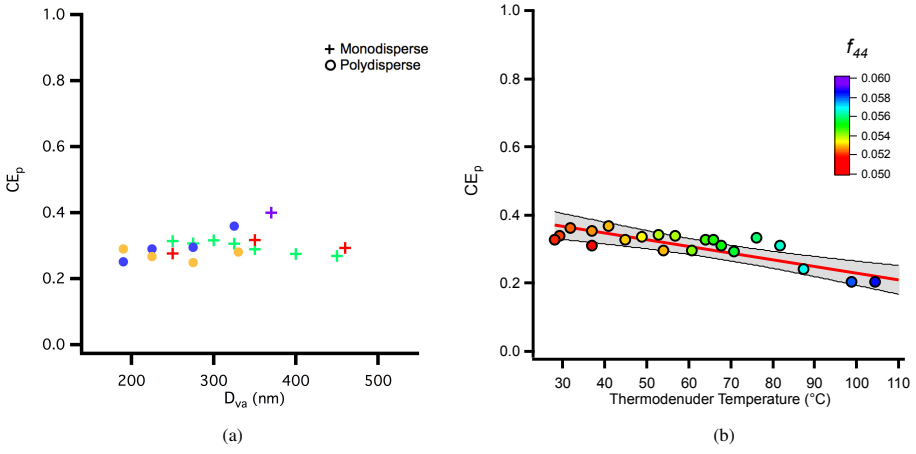

Fig. 11: (a) Particle collection efficiency as a function of D_{va} for all SOA experiments. Data are from both size-selected experiments (crosses) and polydisperse SOA from a smog chamber (circles), with each color representing a separate experiment. (b) Particle collection efficiency for 370 nm size-selected particles (colored markers) as a function of thermodenuder temperature for a single SOA from α-pinene experiment, colored by the fraction of *m/z* 44 (f_{44}) to the total organic mass measured in MS mode. Confidence intervals (95% CI) for a linear fit are shown (slope: -0.0020 $°C^{-1}$).